Interphase Dynamics of photoanode in Micro-energy generation in Photovoltaics

Interphase Dynamics of photoanode in Micro-energy generation in Photovoltaics

T.J. Abodunrin[1], O.O. Ajayi[2], M.E. Emetere[1], A.P.I. Popoola[3], O. Popoola[4], U.O. Uyor[3]

[1] Department of Physics, Covenant University, Ota, Ogun State, Nigeria.
[2] Department of Mechanical Engineering, Covenant University, Ota, Ogun State, Nigeria
3 Department of Chemical, Metallurgical and Materials Engineering, Tshwane University of Technology, Pretoria, South Africa.
4 Department of Electrical Engineering, Centre for Energy and Electric Power, Tshwane University of Technology, Pretoria, South Africa.
Corresponding Author; temitope.abodunrin@covenantuniversity.edu.ng, +2347030380040

Abstract-
Dye-sensitized solar cells (DSCs)as photovoltaics have been subject of intensive research in the last two decades owing to their outstanding features of relative thermal stability, low cost, optical tunability, ability to operate under conditions of poor lighting, and environment friendliness as such, they offer a promising substitute for conventional monocrystalline silicon solar cells. Their poor output efficiency has been incessantly associated with grain boundaries, good quality films are associated with lower recombination decays. and it has been claimed that grain boundaries have a negligible influence on performance. We used microscopy interrelated with scanning electron microscopy to resolve spatially the recombination dynamics from organic films of *Murraya Koenigii*. Stoichiometric organic films, varied in different grains even for the same film. In regions where grain boundaries were dimmer, nonradiative decay occurred faster. Ultraviolet spectroscopy showed positive correlation consistent with photon absorption and regions of the electromagnetic spectrum. The photovoltaic efficiency of *M.Koenigii* DSCs based on TiO2 sensitized with ionic electrolytes was compared. The output efficiency revealed that the ionic potential of Br- was more than 200% value of Cl-, and a final end reaction of above 100% that of I- under similar conditions of atmosphere and experimental set-up.

Key words: Energy harvesting, Electron Occupancy, Affine correction

1. Introduction

In DSSC, photoanode which essentially comprises of a metal oxide semiconducting base is one of most important components for enhancing sunlight absorption, electron excitation and light harvesting efficiency [1]. Photoanode material plays a deterministic role in charge carrier kinematics, dye loading, electron injection, and subsequent power conversion efficiency due to photocurrent and voltage [2]. In view of this, intense research focus is being centered on details of design, chemical composition, structure and morphology of the semiconductor photoanode [3]. Progressive investigations on photoanode type has evolved massive deployment of myriads of photoanode materials such as Nb_2O_5, SnO_2, ZnO, TiO_2, Al_2O_3, graphene, gold and so on [4].

A central theme for this diversity aims at high efficiency output thus, interrelationship of photoanode materials in conjunction with other DSC mechanisms have also become an object

of great scientific work and scrutiny. In effect, morphology, structure and optical properties of metal oxide semiconducting materials remain pertinent subject for research enquiry [5-6].

Influence of ionic strength on thermodynamic environment and properties is also of topmost priority on performance of metal oxides of semiconductors. Inception of instability in colloids, mutual Brownian diffusion quotient of colloidal particles are factors which compete for special attention owing to competition in the choice of particles or ions to be adsorbed. In effect, there is a perceptible decline in particle potential, charge carrier volume and ionic strength between molecular layers. In general, increase in ionic concentration promotes efficient separation into colloidal phases, which accentuates the communal diffusivity, resulting in an appreciable increase in photovoltaic performance [7].

In order to enhance photoelectric output, semiconductors with wide bandgaps are considered. Foremost amongst such photoanode applications are TiO_2 and ZnO nanomaterials because, their wide band gap enables them create highly impressive interfacial, dynamic and structural properties with other DSC components both at room temperature and high sintering experimental conditions [8]. TiO_2 photoanode gained universal acceptability due to availability, low-cost, biocompatibility and non-toxicity. A great significance is attributed to structural isomerism of ZnO photoanode material, encompassing abundant nanostructure morphologies with high electron mobility in nano-particle film and in bulk [9]. In practice, ZnO has a similar conduction band edge and work function relative to TiO_2, but has better charge carrier mobility than TiO_2. This has made ZnO in some instances, become regarded as a more promising photoanode materials for DSCs [10]. Conversely, peculiar problems of ZnO instability in acidic medium, and development of aggregates with dyes on its surface depreciate its photoelectric performances [11]. A faster rate of electron transport rate is directly proportional to reduction in electron-hole recombination rate and enhanced conversion efficiency. Consequently, heterojunction and hybrid photoanodes are being used extensively to counteract the limitations of a monotype photoanode [12]. Some other semiconductor materials have gained influence for their higher photovoltaic ability, examples of such include, Zn2SnO4 which has a more positive conduction band edge position, high versatility and multi-functionality compared to TiO2 [13]. Heterogenous nanomaterials exhibit vast practical and technological applications in light emitting diodes, chemical and gas sensors and present opportunities to re-define optoelectronics, photocatalysis, memory resistors, pyroelectric and piezo-electronic spheres with their optical tunable features [14]. Thus, this study seeks to explore the effect of ionic variation on semiconductor oxide of TiO_2 nanomaterial.

2. Experimental Methods

In standard procedure, 50 g of TiO_2 Degussa of commercial variety, was dissolved in 20 ml of 1.0M conc. trioxonitrate (V) acid and then 3 drops of ethanol were slowly added to the colloidal solution with continuous stirring, to constitute the TiO_2 photoanode. Afterward, the entire reaction mixture was transferred into air tight reagent bottles where they were consequently applied by the doctor blade technique on indium doped tin oxide (ITO) conducting glass. The photoanode was affixed onto the ITO through high temperature sintering at $450^{O}C$ for 1.5 h and allowed to subsequently cool down to room temperature. Dye

solution comprising 1ml: 100 of 1.0M conc. ethanol was sprayed onto the photoanode surface. The counter electrode was fabricated by masking an ITO with epithelial layers of soot over a naked Bunsen flame and then allowed to assume constant temperature. A pair comprising of photoanode and counter electrode were fastened together with binder clips, two drops of different ionic electrolytes constituted by standard practice; 1 g potassium iodide, potassium bromide and potassium chloride dissolved in 100 ml of deionized water was introduced in-between the ITO. This experimental set-up was connected in parallel to variable load and a digital multimeter to obtain readings under standard conditions of 1 atmosphere [15].

3. Results and discussion

Ultraviolet spectroscopy: The vibrionic transitions that occur in *M.Koenigii* molecules being excited by photons of energy is responsible for electronic transitions illustrated by Figure 1. Under standard conditions of 1 atmosphere, at room temperature, the molecule begins from the ground state where energy v = 0, and consequent of absorption of quantized energy, transits to an excited energy state. This new state may cause a shift in the equilibrium of *M.Koenigii* nucleus, re-configuring its electron configuration. In Figure 1, this shift is depicted as different strata, E_0 is the ground, E_1 first excited state and E_2 the highest excitation state. The distinct energy levels are representing different cartesian coordinates, characterized by internuclear separation [16]. A probability of a particular molecule ending up in a definite energy level is proportional to square of the vertical displacement of vibrational wavefunctions of E_1 and E_2 [17]. According to quantum principle, E_2 excited state molecules can rapidly decrease to E_1 vibrational level and decay to E_0, electronic ground state by photon emission. The latter is known as a relaxation process causing the release of phonons, this is a distinctive property of the lattice vibration [18].

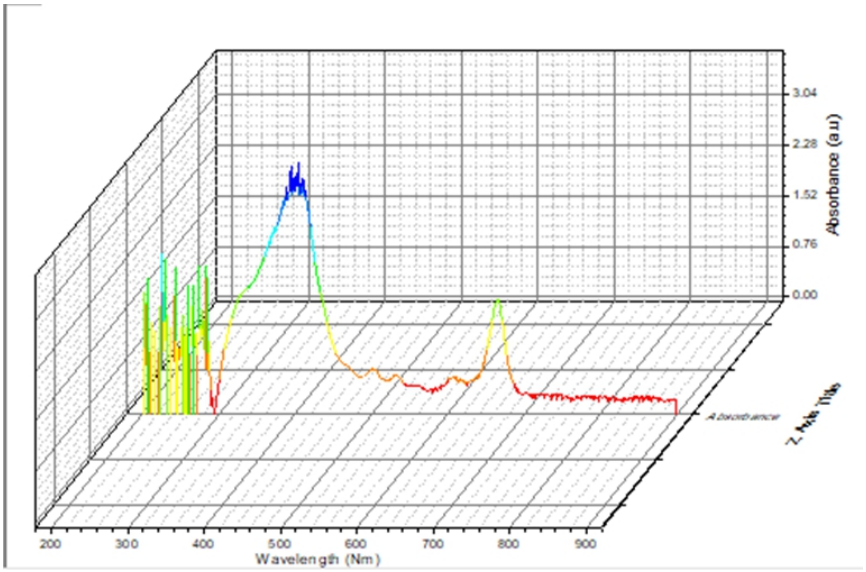

Figure 1**:** Molecular excitation of *M.Koenigii* coordinates with color shades

Scanning Electron Microscopy (SEM): The performance on nanoscale was investigated using scanning electron microscopy with Gwydion software. In Figure 2 (a), electron seats are represented by the red dots, carrier transport is largely by hopping from one seat to the next. A large percentage of the electron seats are present in the mid-section, carrier transport will be higher in this region. At the fringes, the blue zone dominates, region where electron tunneling activities are promoted. Examination of result from surface probe of *M.Koenigii* is illustrated in Figure 2 (b) within φ (x): ± 54.8 which corroborates Figure 2 (a) spectroscopy. Further spectroscopic investigation along the grains of *M.Koenigii* is revealed in Figure 3 (a), the etch observed transversely efficiently separates the mid-section of the micrograph from the boundaries. In order to obtain the coordinate geometry as shown on Table 1 of the grain boundaries, the affine correction was plotted as shown in Figure 3 (b). Figure 3 (a) shows the scalar proportions while Figure 3 (b) presents the vectoral dimensions in *M.Koenigii* nanocomposite.

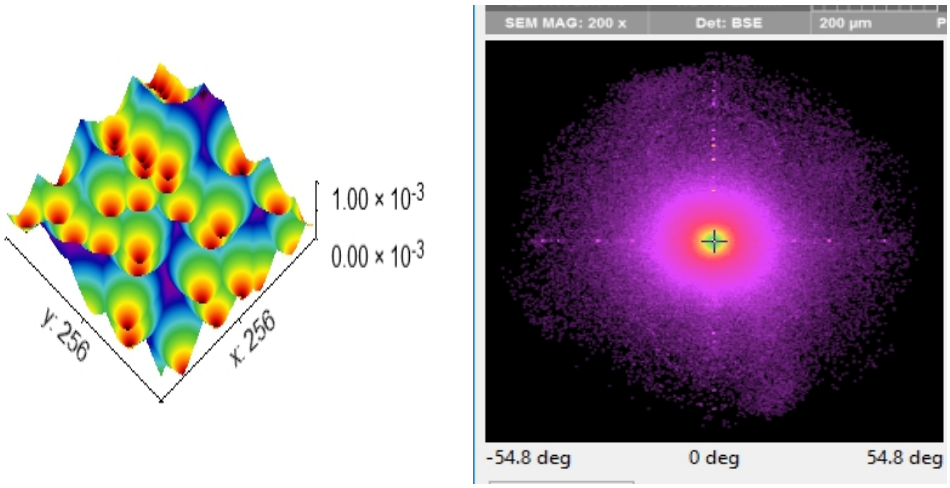

Figure 2 (a): *M.Koenigii* Electron occupancy and (b) Facet Analysis at 3.000 ^{0} tolerance level and facet plane size 3*px*

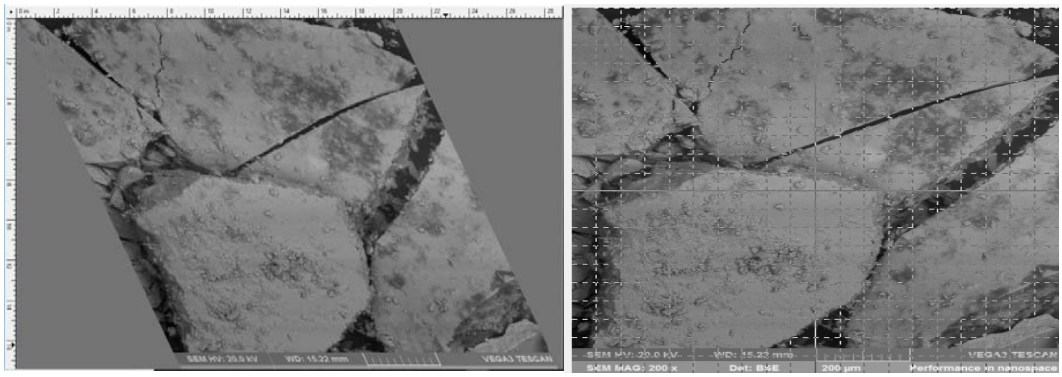

Figure 3 (a): Co-Planar spectroscopy of SEM and (b) Affine Correction of *M.Koenigii*

Table 1: Coordinates of lattice vectors of *M.Koenigii* plotted with Gwydion

Data Process	Lattice Vectors					
Affine Correction	x (µm)		y (µm)	Φ (^{0})	Length(µm)	
	a_1: 5.000		-0.000	-0.00	5.000	
	a_2: 0.000		5.39	90.00	5.391	
Lattice type: $a_1(1)$, φ (2.035^0)	n	Φ (^{0})	φ (^{0})	x(µm)	y(µm)	z(µm)
	1	36.47	169.12	-0.584	0.112	0.804
Estimated Affine Correction	x (m)		y (m)	Length (m)	Angle (^{0})	
	a_1: 1.0000		-0.0000	1.0000	-0.00	
	a2: -0.4481		0.8940	1.0000	116.62	

Magnetic Flux Microscopy in *M.Koenigii*: The current line stray field investigated a graphical simulation of magnetic lines of force distribution in *M.Koenigii* particle with four domains acting under the influence of a field pulsation. These lines correlate with sphere of magnetism which consists of parallel components as depicted by the hue of shades to the long and short sides of the particle and are denoted by full and dashed lines, respectively. In Figure 4(a), a pictorial form of algorithms for stray field calculation using Fourier transform is illustrated. It is used to modify the field from one-layer height to another in multiple modular times to simulate a planar coil shown as two lines with opposite directions of the current. In order to optimize the charge carrier flow, a Hough space of *M.Koenigii* current field line is grouped into uniform sub-sections. The effect is a 2-D lattice defined by parameters along the x and y cartesian coordinate system as shown in Figure 4(b). The result is an average vote for each electric field current line, resulting in the cluster observed which coincides with the pattern of electric flux of *M.Koenigii*.

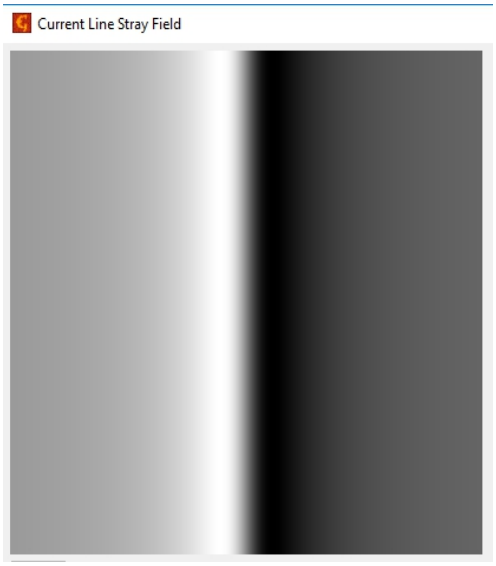

Figure 4:

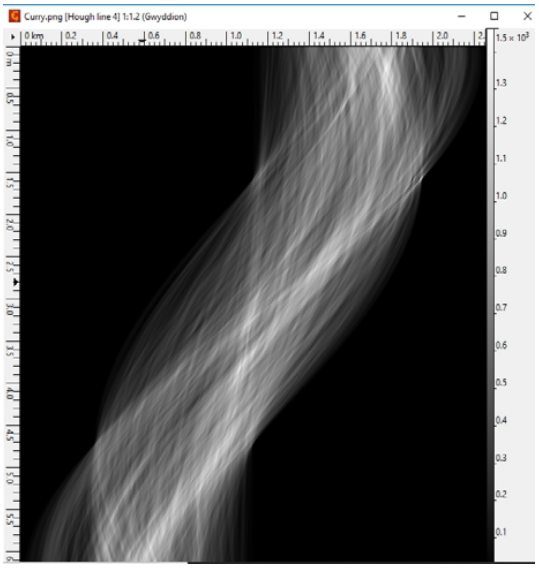

Figure 5: (a): Current line stray field and (b) Hough line of *M.Koenigii*

Photoelectric Evaluation of *M.Koenigii* DSCs: The effect of sensitizing *M.Koenigii* with three different electrolytic solutions comprising Br^-, Cl^- and I^- is illustrated in Figure 5. Under the same operating conditions, the kinematics of the reaction based on similar TiO_2 photoanode nanomaterial, is decidedly disparate. Br^- shows a direct proportional relationship between increase in load and the ionic potential, this is a promising result for suitable application in photosensors. The activation energy required by I^- is very large thus, the reaction kinematics does not favor the transport of I^-. It is notable that the reaction of Cl^- and Br^- was the same at the initial stage then, Br^- was preferred in the redox reaction whereas Cl^- maintained almost the same level of ionic potential.

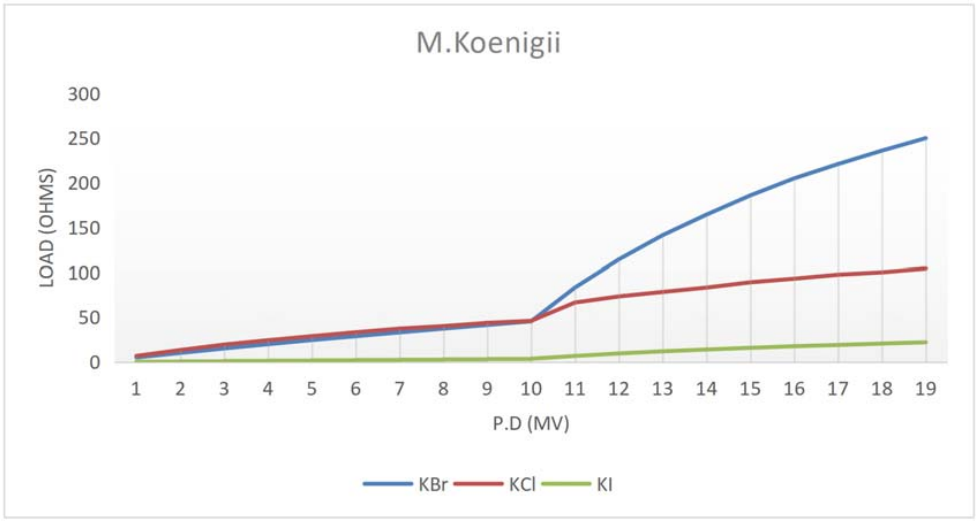

Figure 6: Photoelectric response of *M.Koenigii* DSCs to different ions

4. Conclusions

The use of grain boundary exposed the margin of active reaction in *M.Koenigii* DSCs, Br^- complements molecular kinematics in *M.Koenigii*. A preliminary check provided by the current stray line launches a novel pathway to boost the subsequent output performance of Br^- and every other DSC. Kinematics and Ionization potential of reactions are crucial determinants of charge transport in DSCs, future researches would reveal more insights into these dual phenomena. Also, co-sensitization of the ionic electrolyte sensitizers could be used in future applications on TiO_2 photoanode and hybrid photoanodes for subsequent application in high efficiency optoelectrical devices.

Acknowledgements

The authors wish to acknowledge the financial support offered by Covenant University in actualization of this research work for publication

Reference

[1] Fan, K., Yu, J. & Ho. W. (2017). Improving photoanodes to obtain highly efficient dye-sensitized solar cells: a brief review, Mater. Horiz.,4, 319-344.
[2] Shah, S. A. A., Sayyad, M. H., Wahab, F. & Khan, K. A. (2016). Synthesis, modeling and photovoltaic properties of a benzothiadiazole based molecule for dye-sensitized solar cells, J. Mater. Sci-Mater. El, 27, 4501–4507.
[3] Chandra, S. (2012). Recent trends in high efficiency photo-electrochemical solar cell using dye-sensitized photo-electrodes and ionic liquid based redox electrolytes. P. Natl. A Sci. India A, 82(1), 5–19 (2012).
[4] Abodunrin, T. J. Boyo, A. O. Usikalu, M. R. & Emetere, M. E. (2019). Investigating the Influence of Selective Co-sensitization of Two N719 Dyes on the Micro-Energy Generation from Dye-sensitized Solar Cells. Journal of Physics: Conference Series 1299 (1), 012027.
[5] Vinay, A. I., Jonathon, K. S., Elena, C. M., Nemani, V. P. & Qian, S. Y (2017). Assessing the impact of electrolyte conductivity and viscosity on the reactor cost and pressure drop of redox-active polymer flow batteries, J. Power. Sources 1, 1–11.
[6] Yan, L., Wu, F., Peng, L., Zhang, L., Li, P., Dou, S. & Li, T. (2012). Photoanode of Dye-Sensitized Solar Cells Based on a ZnO/TiO_2 Composite Film, International Journal of Photoenergy, 2012, Article ID 613969.
[7] Ali, N., Hussain, A., Ahmed, R., Wang, M.K., Zhao, C., Haq, B. U. I. & Fu, Y.Q. (2016). Advances in nanostructured thin film materials for solar cell applications, Renewable & Sustainable Energy Reviews, 59: 726–737.

[8] Sengupta, D., Mondal, B. & Mukherjee, K. (2015). Visible light absorption and photo-sensitizing properties of spinach leaves and beetroot extracted natural dyes, Spectrochim Acta A, 14: 85-92.
[9] Wang, L., Wang, Y., Yang, Y., Wen, X., Xiang, H. & Li. Y. (2015). Fabrication of different crystallographically oriented TiO_2 nanotube arrays used in dye-sensitized solar cells, RSC Adv, 5: 41120-41124.
[10] Guo, E. & Yin, L. (2015). Tailored $SrTiO_3/TiO_2$ heterostructures for dye-sensitized solar cells with enhanced photoelectric conversion performance, J. Mater Chem A, 3: 13390-13401.
[11] Kim, H. B., Kim, H., Lee, W.I. & Jang, D.J. (2015). Hierarchical mesoporous anatase TiO_2 nanostructures with efficient photocatalytic and photovoltaic performances, J. Mater Chem A, 3: 9714-9721.
[12] Jia, H-L., Li, S-S., Gong, B-Q. Gu, L., Bao, Z-L. & Guan, M-Y. (2020). Efficient co-sensitization of new organic dyes containing bipyridine anchors with porphyrins for dye-sensitized solar cells, Sustainable Energy & Fuels, 1.
[13] Kim, J.Y., Kwak, G., Choi, Y.C., Kim, D.-H. & Han, Y.S. (2019). Enhanced performance of perovskite solar cells by incorporation of a triphenylamine derivative into hole-transporting poly(3-hexylthiophene) layers. J. Ind. Eng. Chem., 73, 175–181.
[14] Nath, N.C.D. & Lee, J.J. (2019). Binary redox electrolytes used in dye-sensitized solar cells. J. Ind. Eng. Chem., 78, 53–65.
[15] Abodunrin, T.J., Boyo, A.O. & Usikalu, M.R. (2018). The interboundary properties and kinematics of N719 dye with titania photoanode framework and spectral responses with different electrolytes, Cogent Physics, 5 (1), 1-11.

[16] Arkan, F., Izadyar, M. & Nakhaeipour, A. (2016). The role of the electronic structure and solvent in the dye-sensitized solar cells based on Zn-porphyrins: Theoretical study, Energy, 114, 559–567.
[17] Khan. F. U. (2016). Energy Harvesting from the Stray Electromagnetic Field around the Electrical Power Cable for Smart Grid Applications, The Scientific World Journal, Article ID 3934289.
[18] Ye, H., Shang, G., Wang, L. & Zheng, M. (2015). A new method based on hough transform for quick line and circle detection, 2015, 8th International Conference on Biomedical Engineering and Informatics (BMEI), 52-56.